Initial Excited-State Structural Dynamics of 5,6-Dimethyluracil from Resonance Raman Spectroscopy

ARTICLE *in* THE JOURNAL OF PHYSICAL CHEMISTRY A · JUNE 2014

Impact Factor: 2.69 · DOI: 10.1021/jp412747c · Source: PubMed

2 AUTHORS, INCLUDING:

Swaroop Sasidharanpillai
University of Guelph
3 PUBLICATIONS **4** CITATIONS

THE JOURNAL OF PHYSICAL CHEMISTRY A

Article

pubs.acs.org/JPCA

Initial Excited-State Structural Dynamics of 5,6-Dimethyluracil from Resonance Raman Spectroscopy

Swaroop Sasidharanpillai and Glen R. Loppnow*

Department of Chemistry, University of Alberta, Edmonton, Alberta, Canada T6G 2G2

ABSTRACT: In order to understand the effect of methyl substitution patterns on the initial excited-state structural dynamics of uracil derivatives, we measured the resonance Raman spectra of 5,6-dimethyluracil (5,6-DMU). The results show that the resonance Raman spectrum is a combination of that of 5-methyl- and 6-methyluracil. The resonance Raman excitation profiles (RREPs) and absorption spectrum are simulated with a self-consistent, time-dependent formalism to yield the excited-state slopes and broadening parameters. The initial excited-state structural dynamics occur primarily along the C5═C6 stretching mode, as expected, but with lesser excited-state slopes along each mode compared to 5-methyluracil and 6-methyluracil. This study along with previous experiments with different uracil derivatives show that the presence and positions of the methyl groups seems to determine the partitioning of initial excited-state structural dynamics.

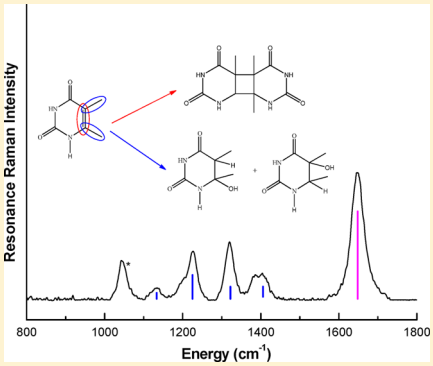

INTRODUCTION

The difference between DNA and RNA arises from two factors: the difference in the sugar—the pentose sugar is deoxyribose in DNA and ribose in RNA—and the difference in one of the nucleobases. While adenine, guanine, and cytosine are found in both DNA and RNA, thymine is only found in DNA and uracil only in RNA. The only difference between thymine and uracil is the presence of a methyl group at the C5 position of thymine instead of the hydrogen in uracil as shown in Scheme 1.

Scheme 1. Structure of Different Uracil Derivatives

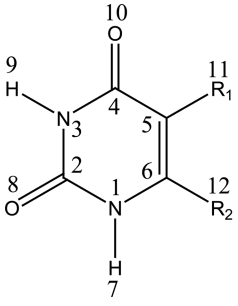

R_1	R_2	Compund
H	H	Uracil (U)
CH_3	H	Thymine (T or 5-MU)
H	CH_3	6-methyluracil (6-MU)
CH_3	CH_3	5,6-dimethyluracil (5,6-DMU)

The photochemistry of thymine and uracil nucleobases differ from one another.[1,2] Thymine forms the cyclobutyl pyrimidine dimer (CPD) as the major photoproduct upon UV irradiation, whereas the photohydrate is the major photoproduct in uracil.[1,2] Only a good understanding of the initial excited-state *structural* dynamics of the molecules can help us rationalize the reason for this difference in photochemistry.

Much work has been done on the *electronic* excited-state dynamics of the nucleobases, primarily with femtosecond transient absorption and fluorescence spectroscopy.[3−13] Singlet excited states of thymine and uracil decay on the femtosecond time scale.[3−5] Excited-state lifetimes of <100 and 540 fs were found for uracil and thymine from fluorescence lifetime studies[3] and femtosecond transient absorption spectroscopy.[3,5] The increase in the excited-state lifetime of thymine compared to uracil has been attributed to C5 pyramidalization.[3] These very fast relaxation times result from ultrafast internal conversion.[4,5] Gustavsson et al. looked at the singlet excited-state dynamics of the pyrimidine nucleobases and their derivatives in different solvents with femtosecond fluorescence upconversion spectroscopy and found that all of them decay on a femtosecond time scale.[3,12] Phillips et al. employed femtosecond time-resolved fluorescence and transient absorption spectroscopy to study thymidine and thymine oligonucleotides and found an ultrafast, single base-localized, stepwise mechanism that deactivates the thymine multimer.[13] However, all these excited-state dynamics measurements provide very little insight into the structural changes in the excited state.

Resonance Raman spectroscopy has been used to probe the initial excited-state *structural* dynamics of the nucleobases.[14−19] Loppnow et al. used resonance Raman spectroscopy to measure the initial excited-state structural dynamics of thymine and uracil and found that they are different from one another.[14,15] Most of the initial excited-state dynamics of uracil is directed along C5H and C6H bending modes, whereas they are oriented along both CH bending and C5C6 stretching modes in thymine. Similarity between the initial excited-state structural dynamics of 5-methyluracil (5-MU) and 5-fluorouracil (5-FU) and the similarity of the structural dynamics of 5-deuterouracil (5-d-U) to both 5-MU and uracil strongly suggests that the mass of the C5 substituent dictates the initial excited-state

Received: December 30, 2013
Revised: May 25, 2014
Published: June 1, 2014

   dx.doi.org/10.1021/jp412747c | J. Phys. Chem. A 2014, 118, 4680−4687

structural dynamics of different uracil derivatives.[16−18] Surprisingly, further studies with methyl substitution at the C6 position of uracil show that partitioning of the initial excited-state structural dynamics between the CH bending and stretching modes is different than thymine; 6-methyluracil has less structural distortion along the CH bending modes, though the initial excited-state structural dynamics along the C5═C6 stretching mode in C5 and C6 methyl-substituted uracil are similar.[18]

To further understand the effect of structure on the initial excited-state structural dynamics, we studied the initial excited-state structural dynamics of 5,6-dimethyluracil (5,6-DMU, Scheme 1) in this paper. This uracil derivative has similar masses at the C5 and C6 position, but the C5 and C6 hydrogens of uracil are replaced by methyl groups. The presence of a methyl group at both C5 and C6 positions therefore will help to differentiate the role of the C5 and C6 positions and the mass effect in determining the initial excited-state structural dynamics.[18]

EXPERIMENTAL SECTION

5,6-Dimethyluracil (2,4-dihydroxy 5,6-dimethylpyrimidine, Sigma-Aldrich, Oakville, Ontario) and sodium nitrate (99%, EMD Chemicals Inc., Gibbstown, NJ) were used without any further purification. Solutions were prepared with nanopure water from a Barnstead water filtration system (Boston, MA).

UV resonance Raman spectra were measured as described previously.[14,20−22] The concentration of 5,6-dimethyluracil was 4−5 mM, and the sodium nitrate internal standard concentration was 0.3 M. The actual concentration during the experiment was monitored by measuring the absorption spectrum before and after each resonance Raman experiment using a diode array absorption spectrometer (Hewlett-Packard 8452, Sunnyvale, CA). All resonance Raman spectral measurements were done in triplicate. Resonance Raman frequencies for 5,6-dimethyluracil reported here are accurate to ±5−10 cm^{-1}. For the depolarization ratio measurements, a UV-transparent polarizing beam splitter cube was introduced into the collection optics between the sample and the spectrometer and the spectrum measured as for the nonpolarized spectra. The perpendicular and parallel polarizations were calibrated using a 0.3 M solution of sodium nitrate (ρ = 0.04).

The overtone and combination band region for 5,6-dimethyluracil at 257 nm was recorded using a UV Raman microscope (Renishaw, Chicago, IL) as described previously.[14] A solution of 5 mM 5,6-dimethyluracil and 0.3 M nitrate in a small beaker was constantly moved using a translation stage to minimize photodegradation of the sample. The 1332 cm^{-1} vibration of diamond was used to calibrate the frequencies. Resonance Raman spectra in the overtone and combination band region were repeated with three sets of fresh samples.

The absolute resonance Raman cross sections were calculated from the integrated band intensities using the following equation

$$\left(\frac{d\sigma_R}{d}\right)_{5,6DMU} = \left(\frac{d\sigma_R}{d}\right)_{IS} \cdot \frac{I_{5,6DMU}}{I_{IS}} \cdot \frac{[IS]}{[5,6DMU]} \cdot \frac{L_{5,6DMU}}{L_{IS}} \cdot SA \quad (1)$$

where $d\sigma_R/d\Omega$ is the differential resonance Raman cross-section of the vibrational mode, $I_{5,6DMU}$ and I_{IS} are the integrated band intensities of the 5,6-dimethyluracil and the internal standard, respectively, [IS] and [5,6-DMU] are the concentrations of internal standard and the 5,6-dimethyluracil, respectively, $L_{5,6DMU}$ and L_{IS} are the standard lamp efficiency for the 5,6-dimethyluracil and the internal standard vibrational frequencies, respectively, and *SA* is the differential self-absorption of the resonance Raman scattered light at the 5,6-dimethyluracil and internal standard vibrational frequencies. Details of converting the resonance Raman intensities to differential resonance Raman cross-section have been described previously.[20−22] The internal standard resonance Raman differential cross-sections for nitrate used for the calculations were 3.68×10^{-11}, 2.43×10^{-11}, 1.53×10^{-11}, $1.02 \times 10^{-11,}$ and 8.37×10^{-12} $Å^2$ $molecule^{-1}$ sr^{-1} at 250, 257, 266, 275, and 280 nm, respectively.

Resonance Raman Structural Dynamics. The resonance Raman differential cross-sections as a function of excitation wavelength (excitation profiles) and the absorption spectrum of 5,6-dimethyluracil were simulated with a time-dependent formalism as described previously[20,22]

$$\sigma_R(E_L) = \frac{8\pi E_s^3 E_L e^4 M^4}{9\hbar^6 c^4} \int_0^\infty dE_0 H(E_0) \left| \int_0^\infty dt \langle f|i(t)\rangle \exp\left\{\frac{i(E_L + \varepsilon_i)t}{\hbar}\right\} G(t) \right|^2 \quad (2)$$

$$\sigma_A(E_L) = \frac{4\pi E_L e^2 M^2}{6\hbar^6 cn} \int_0^\infty dE_0 H(E_0) \int_{-\infty}^\infty dt \langle i|i(t)\rangle \exp\left\{\frac{i(E_L + \varepsilon_i)t}{\hbar}\right\} G(t) \quad (3)$$

where E_L and E_S are the energies of the incident and scattered photons, respectively, M is the transition length, n is the refractive index, ε_i is the energy of the initial vibrational state, $|i\rangle$ and $|f\rangle$ are the initial and final vibrational wave functions in the Raman scattering process, respectively, $H(E_0)$ is the normalized inhomogeneous distribution of the zero−zero energies around an average zero−zero energy ($\bar{E}_0$), $|i(t)\rangle$ is the initial ground vibrational wave function propagated on the excited-state potential energy surface, and $G(t)$ is the homogeneous line width function, which represents the dynamics of chromophore−solvent coupling within the high-temperature limit of the Brownian oscillator model.[23] Within the harmonic oscillator approximation, the $\langle i|i(t)\rangle$ and $\langle f|i(t)\rangle$ overlaps depend only on the slopes ($\beta/\hbar$) of the excited-state potential energy surface at the ground-state equilibrium geometry along each normal mode of vibration. Implementation of these equations has been described in detail previously.[16,20−24] The self-consistent simulation of the absorption spectrum and resonance Raman excitation profiles has been performed as previously described.[19,23] For analysis, the parameters were adjusted so as to get good agreement between the experimental and simulated absorption spectra and the resonance Raman excitation profiles. The overtones and combination bands were used as additional constraints to optimize the parameters. Mode assignments were obtained from a density functional theory (DFT) calculation at the B3LYP/6-311G (d,p) level of theory using the Gaussian09 package to find the minimum energy structure followed by conversion of internal coordinates from Cartesian to symmetry coordinates with the GAR2PED package.[25,26]

RESULTS

Figure 1 shows the resonance Raman spectra of 5,6-DMU excited at different wavelengths (280, 275, 266, 257, and 250 nm) within the 260 nm absorption band. Peaks are observed at 475, 635, 1135, 1225, 1310, 1410, and 1665 cm^{-1}. The relative intensities of the peaks remain the same at different excitation wavelengths, and no change in frequencies for the modes are observed. This observation indicates that the resonance enhancement results from a single electronic transition within the 260 nm absorption band. The two less intense peaks at 475 and 1135 cm^{-1} are not observed at all excitation wavelengths due to difficulties in differentiating them from the background at some excitation wavelengths.

The resonance Raman spectrum of 5,6-DMU at 257 nm is compared to the resonance Raman spectra of other uracil derivatives at the same excitation wavelength in Figure 2. The resonance Raman spectra in Figure 2 show a gradual change in

dx.doi.org/10.1021/jp412747c | J. Phys. Chem. A 2014, 118, 4680−4687

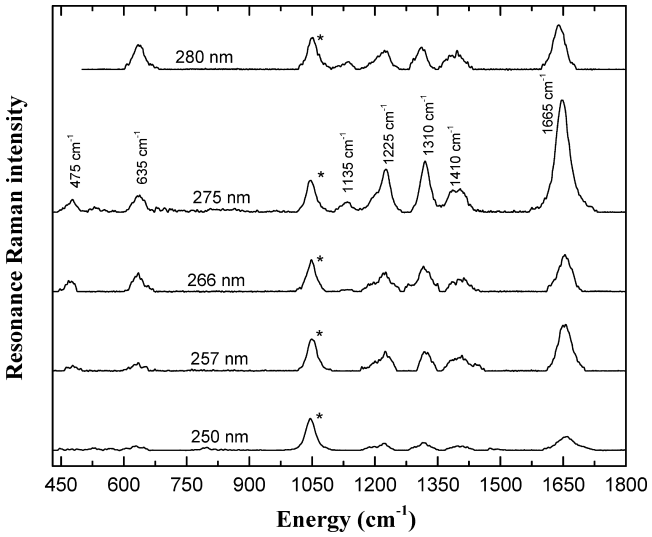

Figure 1. Resonance Raman spectra of 5,6-DMU excited at different wavelengths throughout the 260 nm absorption band. The concentration of 5,6-dimethyluracil was ~5 mM, and that of the nitrate internal standard was 0.3 M. The internal standard peak is denoted by an asterisk (*). All spectra are normalized with respect to the internal standard peak.

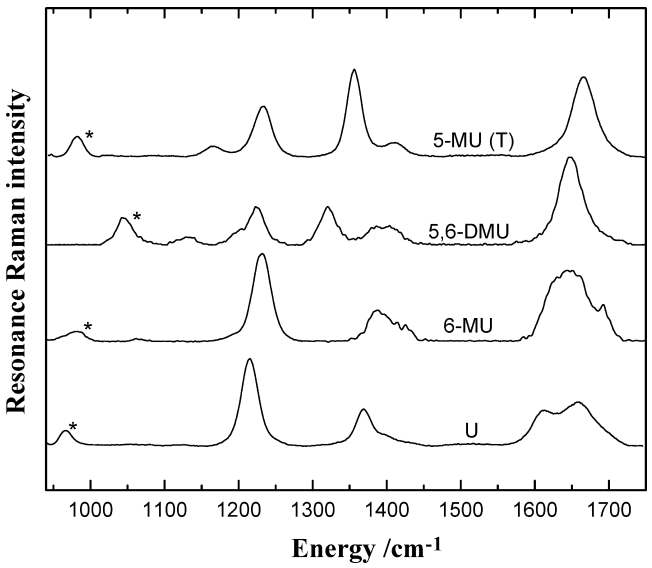

Figure 2. Resonance Raman spectra of different uracil derivatives excited at 257 nm. The internal standard peak is denoted by an asterisk (*). For uracil (U), 6-methyluracil (6-MU), and 5-methyluracil (5-MU, T) the internal standard was sulfate, and for 5,6-dimethyluracil (5,6-DMU) the internal standard was nitrate.

spectral features on going from uracil to thymine. The peak around 1230 cm^{-1} is seen in all the uracil derivatives, with its relative intensity decreasing from U to 6-MU to 5,6-MU to 5-MU. A single peak is observed at 1388 cm^{-1} in uracil which appears as two peaks at ca. 1350 and 1400 cm^{-1} in methyl-substituted uracil derivatives. The relative intensities of these two peaks change on going from 6-MU to 5-MU to 5,6-DMU. The two peaks are well separated in both 5-MU and 5,6-DMU but shifted to lower wavenumber. The peak around 1660 cm^{-1} is observed in all methyl-substituted uracil derivatives but shifted to 1623 cm^{-1} in uracil. The carbonyl stretch around 1660 cm^{-1} is seen in uracil and may also be a part of the broad band in 6-MU. The 5,6-DMU resonance Raman spectrum can be considered as a combination of the thymine and 6-MU spectra with an additional peak at 1135 cm^{-1} if we allow for the change in frequencies of some of the modes which probably arises from somewhat different normal mode descriptions (see below). The depolarization ratios at 266 nm have been measured for the four most intense modes. The results are depolarization ratios of 0.30 ± 0.06 at 1665 cm^{-1}, 0.32 ± 0.06 at 1410 cm^{-1}, 0.30 ± 0.06 at 1310 cm^{-1}, and 0.28 ± 0.06 at 1225 cm^{-1}, all close to the 1/3 value expected for resonance with a single electronic state.

The presence of methyl groups at both the C5 and the C6 positions in 5,6-DMU results in different relative mode intensities and frequencies compared to thymine (5-MU) and 6-MU (Figure 2). The main peaks in the fingerprint region (1000−1660 cm^{-1}) are seen in all three methyl derivatives of uracil, though the intensities of the peaks and their mode assignments differ (see below). The 5,6-DMU peak at 1225 cm^{-1} has the lowest relative intensity compared to the other two derivatives. The relative intensities of the peaks at 1310 and ca. 1400 cm^{-1} in 5,6-DMU are intermediate between those of 5-MU and 6-MU. The peak around 1660 cm^{-1} in 5,6-DMU is very similar to that of 5-MU and 6-MU in intensity and more intense than that of uracil. To understand these results, we need to have robust vibrational assignments of the normal modes in these derivatives.

A complete mode description and the potential energy distribution for different uracil derivatives are given in Table 1. The resonance Raman spectrum of uracil has peaks at 1235 cm^{-1} resulting from a combination of ring stretching and hydrogen bending modes. A ring stretching mode is observed at 1388 cm^{-1}, the C5═C6 mode at 1623 cm^{-1}, and the carbonyl stretch at 1664 cm^{-1}.[15]

In 6-methyluracil, the peaks at 1235 and 1361 cm^{-1} are assigned to a combination of ring stretch and the hydrogen bending modes.[18] The 1397 cm^{-1} mode is mainly due to the ring stretches. The intense mode at 1660 cm^{-1} in 6-MU is mainly due to the C═C stretch, as in all the uracil derivatives.

Thymine has five intense bands in the 1000−1700 cm^{-1} range, and their assignments are given in Table 1.[14] The peak at 1173 cm^{-1} is mainly due to ring stretch and in-plane hydrogen bending. The intense band at 1237 cm^{-1} is attributed to the C5-methyl stretch mixed with a ring stretch and bend. The C−H bend of C6 is seen at 1362 cm^{-1}. The 1423 cm^{-1} mode is mainly due to a ring stretch.[14] The 1667 cm^{-1} mode in thymine is due to the C5═C6 stretch and the C6H12 bend.

The 257 nm excited resonance Raman spectrum of 5,6-DMU has five intense modes at 1135, 1225, 1310, 1410, and 1665 cm^{-1} assigned in Table 2. The 1135 cm^{-1} peak in 5,6-DMU is assigned to a CH_3 deformation mixed with a ring stretch, the 1225 cm^{-1} peak has contributions from C5C11 and C6N1 stretches, the band at 1320 cm^{-1} of 5,6-DMU is mainly due to the N1H bend mixed with ring stretches, CH_3 deformations are the main contributors to the 5,6-DMU peak at 1410 cm^{-1}, and the most intense mode at 1665 cm^{-1} is mainly due to the C5═C6 stretch.

It is very clear from Tables 1 and 2 that the presence of methyl groups at the C5 and/or C6 positions of uracil change the potential energy distribution (PED) of different modes. Thus, the comparison of modes and the PEDs given in Tables 1 and 2 are not a good comparison of the initial excited-state structural dynamics.

dx.doi.org/10.1021/jp412747c | J. Phys. Chem. A 2014, 118, 4680−4687

Table 1. Harmonic Mode Parameters of 5-MU, 6-MU, and Uracil

mode (cm^{-1})	mode assignments[a]	$\beta/\hbar$ (cm^{-1})
uracil (U)		
579	ring def 3 [32], be(C2O8) [−23], be(C4O10) [−18], ν(C4C5) [−6], ν(C6N1) [6]	266
789	ν(C4C5) [28], ν(N1C2) [19], ring def 1 [13], ν(N3C4) [10], ring def 3 [7], ν(C2N3) [6], ν(C6N1) [6]	379
1235	be(C5H11) [33], be(C6H12) [18], ν(C6N1) [−15], be(N1H7) [10], ν(N3C4) [7], ν(N1C2) [5]	914
1388	ν(C2N3) [18], be(N3H9) [17], ν(N1C2) [15], be(C5H11) [13], be(C6H12) [−12], ν(C5C6) [−8], be(C4O10) [5]	625
1623	ν(C5C6) [61], be(C6H12) [−14], ν(C6N1) [−8]	487
1664	νC4O10) [71], ν(C4C5) [−8], ring def 2 [5]	998
6-methyluracil (6-MU)		
520	ring def 2 [54], ring def 3 [−30]	140
550	γ(C6C12) [28], γ(N1H7) [21], γ(C2N3) [11], ring def 6 [10], γ(C4O10) [9], γ (C5H11) [8]	140
605	be(C2O8) [35], be(C4O10) [35], be(C6C12) [−14]	160
657	γ(C2N3) [75], γ(C6C12) [−8], ring def 4 [−7]	110
1235	be(C5H11) [22], γ(C2N3) [17], ν(N3C4) [−17], ν(N1C2) [−9], ν(C4C5) [8]	590
1361	be(C5H11) [34], be(N1H7) [−26], ν(C2N3) [-7], ν(N1C2) [6]	180
1397	ν(C2N3) [21], ν(N1C2) [−11], be(C2N3) [10], be(C4O10) [−8], ring def 3 [8], ν(C4O10) [−8], ν(C4C5) [−8], ν(C2O8) [6]	410
1660	ν(C5C6) [60], ν(C6C12) [−6]	850
thymine (5-MU)		
567	γ(N1H7) [90], γ(N3H9) [−6]	136
641	be(C4O10) [28], be(C2O8) [−27], be(C5C11) [14], ring def 2 [6]	192
762	γ(C2O8) [60], ring def 6 [−12], ring def 4 [8], γ(C4O10) [6], γ(N3H9) [−5]	229
811	ring def 1 [45], ν(C5H11) [20], ν(N1C2) [−11]	227
1173	ν(C2N3) [21], be(C6H12) [20], be(N1H7) [−16], ν(N3C4) [−12], v(C6N1) [−11]	282
1237	ν(C5C11) [29], ν(C6N1) [−21], ring def [−12], ν(N1C2) [−10], ν(C4C5) [−10], ν(C2N3) [8]	544
1362	be(C6H12) [42], ν(C5C6) [12], ν(N1C2) [9], ν(C2N3) [−9]	681
1423	ν(C2N3) [15], ν(C4C5) [13], CH_3 umb [−11], be(N1H7) [9], ν(N1C2) [−8], be(C4O10) [7], be(C2O8) [7], ring def 2 [−6], be(N3H9) [6]	313
1667	ν(C5C6) [61], be(C6H12) [−13], ν(C6N1) [−8], ν(C5H11) [−5]	917

[a]Frequencies and mode assignments were obtained from refs 14, 18, and15 for 5-MU, 6-MU, and U, respectively. [b]Abbreviations: ν, stretching; def, deformation; γ, out-of-plane bending; be, in-plane bending; umb, umbrella motion of the methyl group.

Table 2. Harmonic Mode Parameters of 5,6-Dimethyluracil

mode[a] (cm^{-1})	mode assignments[b]	$\beta/\hbar$ (cm^{-1})
475	ring def 2 [70], ν(C5C11) [−7], ν(C4N3) [−6]	58
635	be (C4O10) [28], be(C2O8) [−27], −be(C6C12) [14], be(C5C11) [12]	76
1135	CH_{3a} def 4 [22], ν(C6C12) [−17], ν(C4N3) [12], CH_{3a} def 3 [7], ν(C2N3) [−7], be(C5C11) [7]	110
1225	ν(C5C11) [28], ν(C6N1) [−28], ring def 1 [−9], ν(C5C4) [−9], ν(C2N1) [9]	180
1320	be(N1H7) [18], ν(C2N3) [13], ν(C2N1) [−10], ν(C5C4) [9], be(C5C11) [6], ν(C6N1) [−5], ν(C6C12) [5]	190
1410	CH_{3b} def 1 [57], CH_{3a} def 1 [−17], ν(C6C12) [6]	180
1665	ν(C6C5) [62], ν(C6C12) [−5]	340

[a]Frequencies listed here are experimental frequencies. [b]Abbreviations: ν, stretching; def, deformation; be, in-plane bending. Slopes of the excited-state potential energy surface at the Franck−Condon geometry ($\beta/\hbar$) were obtained by fitting the experimental resonance Raman cross sections and absorption spectrum with the following parameters in eqs 2 and 3: temperature, T = 298 K, zero−zero energy, E_0 = 36 800 cm^{-1}, Gaussian homogeneous line width, Γ_G = 1000 cm^{-1}, inhomogeneous line width, θ = 1500 cm^{-1}, transition length, M = 0.675 Å, and Brownian oscillator line shape, $\kappa = \Lambda/D$ = 0.1.

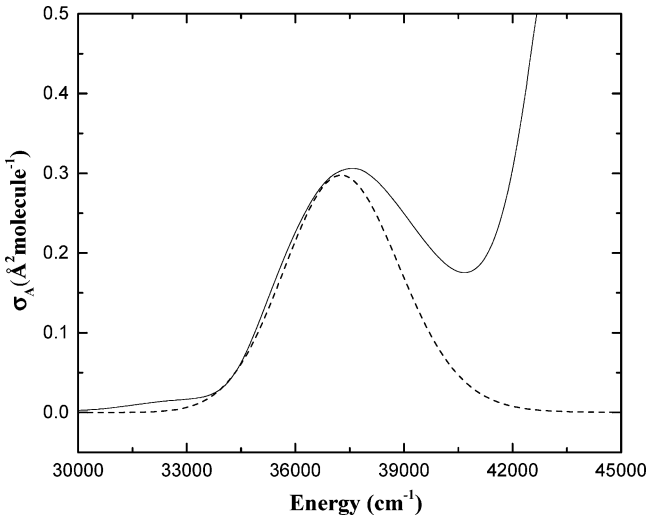

Figure 3. Calculated (dashed line) and experimental (solid line) absorption spectrum of 5,6-dimethyluracil. The simulated absorption spectrum was generated using eq 3 and the parameters of Table 2. The differences between the experimental and the simulated spectra at higher energies than 38 000 cm^{-1} and lower energies than 33 000 cm^{-1} are due to other energy transitions which are not modeled in the equation.

The experimental and simulated absorption spectra of 5,6-dimethyluracil are shown in Figure 3. The experimental absorption spectrum and resonance Raman excitation profiles were simulated by adjusting the parameters in eqs 2 and 3 to get the best agreement between the experimental and the simulated spectra. The deviation between the experimental and the calculated absorption spectra at energies above 38 000 cm^{-1} is due to the fact that the higher energy electronic absorptions are not modeled in the simulation. Also, the discrepancies below 35 000 cm^{-1} may be coming from other possible lower energy transitions in 5,6-DMU, which are also not modeled in the simulation.

The experimental and simulated resonance Raman excitation profiles are shown in Figure 4. The simulated resonance Raman excitation profiles reproduce the experimentally measured resonance Raman cross sections well. The heights of the respective resonance Raman excitation profiles reflect the relative intensities of the peaks in the resonance Raman spectra in Figure 1 and the excited-state slopes ($\beta/\hbar$) along each vibrational mode. The agreement between the experimental and simulated absorption spectra and the resonance Raman excitation profiles indicate that the excited-state parameters obtained from the simulation are accurate. The calculated excited-state slopes, other fitting parameters, and the potential energy distributions for different peaks of 5,6-DMU are tabulated in Table 2.

To better constrain the parameters used for simulation of the absorption spectrum and the resonance Raman excitation

dx.doi.org/10.1021/jp412747c | J. Phys. Chem. A 2014, 118, 4680−4687

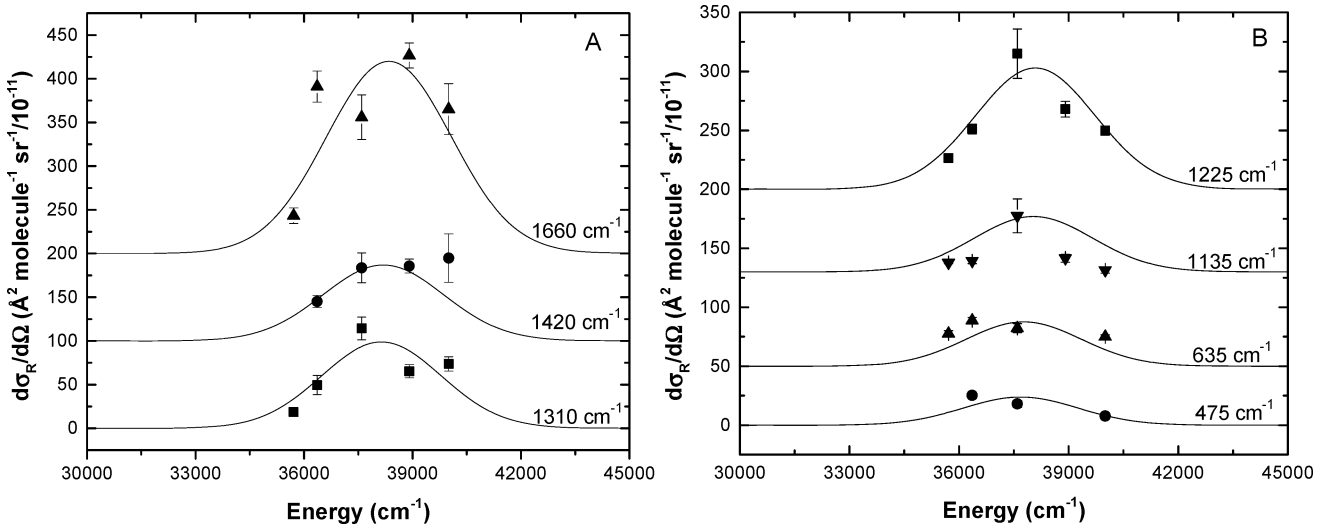

Figure 4. Experimental (points) and calculated resonance Raman excitation profiles (solid line) for 5,6-dimethyluracil at high wavenumbers (A) and low wavenumbers (B). Excitation profiles were calculated using eq 2 and the parameters of Table 2.

profiles, the overtones and combination bands between 1700 and 3000 cm^{-1} were also measured at 257 nm. The overtone and combination bands above 3000 cm^{-1} were obscured by the broad O−H stretching vibrations of water. The experimental and predicted overtones and combination bands for 5,6-DMU are given in Table 3. Most of the calculated overtone and combination band intensities are in agreement with the observed intensities within the experimental error. The higher degrees of error in the experimental overtone and combination band cross sections compared to the fundamental cross sections are due to both their lower intensity and additional observed imprecision arising from focus-dependent intensities in the Raman microscope. The agreement between the experimental and the calculated cross sections ensures the accuracy of the parameters used to simulate the absorption spectrum and resonance Raman excitation profiles.

Table 3. Experimental and Calculated Resonance Raman Cross Sections for Overtone and Combination Bands of 5,6-Dimethyluracil (5,6-DMU)

mode (cm^{-1})[a]	mode assignment	$d\sigma_{expl}/d\Omega$ (Å^2 molecule^{-1} sr^{-1}/ 10^{-11})	$d\sigma_{calcd}/d\Omega$ (Å^2 molecule^{-1} sr^{-1}/ 10^{-11})
2958	1320 + 1665	4.2 ± 0.8	5.3
2864	1225 + 1665	4.5 ± 0.9	5.3
2706	1135 + 1665, 1320 + 1410	4.1 ± 1.3	4.6
2624	1225 + 1410, 2 × 1320	2.7 ± 0.8	3.6
2530	1225 + 1320, 1135 + 1410	2.4 ± 1.4	3.7
2446	1135 + 1320, 2 × 1225	2.1 ± 1.0	2.6
2379	1135 + 1225	1.5 ± 0.25	1.3
2276	635 + 1665, 475 + 1665, 2 × 1135	5.5 ± 1.8	3.6
1953	635 + 1320, 635 + 1410	2.5 ± 1.1	1.6
1864	475 + 1320, 475 + 1410, 635 + 1225	2.6 ± 0.6	2.0

[a]Frequencies listed are experimental frequencies. Cross sections were calculated using eq 2 and the parameters in Table 2. Experimental cross sections were calculated from the resonance Raman spectra of overtone and combination bands of 5,6-DMU at 257 nm.

Table 4 compares the electronic and broadening parameters for the different uracil derivatives. The zero−zero energy, transition length, and total broadening are similar in all uracil derivatives, within experimental error, except for the zero−zero energy for 5-MU. The difference in the zero−zero energy between 5-MU and 5,6-DMU is evident from the experimental absorption spectrum as well. Another model with homogeneous and inhomogeneous broadening similar to the other uracil derivatives was tried and not considered any further due to inconsistently large calculated overtone and combination band cross sections compared to those experimentally measured.

Table 4. Comparison of Harmonic Parameters of Different Uracil Derivatives[a]

	5-MU	5,6-DMU	6-MU	U
E_0 (cm^{-1})	35 650	36 800	36 700	36 500
M (Å)	0.67	0.68	0.72	0.65
Γ_G (cm^{-1})	1700	1000	1470	1450
θ (cm^{-1})	1075	1500	1040	1000

[a]The parameters for 5-MU, 6-MU and U were obtained from references 14, 18, and 15, respectively. E_0 is the zero−zero energy, M is the transition length, Γ_G is the homogeneous line width and θ is the inhomogeneous line width.

DISCUSSION

The results presented here continue our exploration of how molecular structure influences excited-state initial structural dynamics in pyrimidine nucleobases. Most mechanisms of excited-state electronic dynamics and relaxation in pyrimidine nucleobases, with uracil as the simplest of those, have come from computational studies.[27] Although still contentious due to the lack of experimental data, three conical intersections have been identified, the earliest one on the S_2 ($\pi\pi^*$) state being one that putatively involves a C5═C6 twisting motion to reach.[27] The results here clearly show that both C5═C6 stretching and in-plane bending is important in the first few femtoseconds on the S_2 surface, somewhat consistent with such a model. In

dx.doi.org/10.1021/jp412747c | J. Phys. Chem. A 2014, 118, 4680−4687

Table 5. Comparison of Reorganization Energy along Different Internal Coordinates for Different Uracil Derivatives

	ring str	ring def	C4O10 str	C5C6 str	C5 bend	C6 bend	bend	active
U	21%	5%	21%	6%	13%	9%	22%	27%
6-MU	21%	2%	1%	26%	7%	5%	12%	38%
5-MU	16%	5%	0%	24%	8%	15%	23%	48%
5,6-DMU	14%	5%	0%	25%	11%	13%	24%	48%

Reorganization energy was calculated using eq 4. Reorganization energies do not add up to 100% due to neglecting internal coordinate contributions < 5% PED in Tables 1 and 2. Abbreviations: str, stretching; def, deformation; bend, in-plane bend; active, photochemically active coordinate. For the C=C stretching internal coordinate, only the C5=C6 stretch contribution was considered, and for the in-plane internal coordinate, C5H, C5C11, C6H, and C6C12 bends and CH_3 deformations, as appropriate, were considered. Ring stretch refers to any stretch along the ring other than the C5=C6 bond, and ring deformation refers to different ring def (ring def 1, ring def 2, etc.) described in Tables 1 and 2.

thymine, the photochemical reaction to form the CPD photoproduct occurs along a barrierless trajectory from the Franck−Condon region, provided the conformations of the two thymine nucleobases with respect to one another are favorable for CPD formation.[28] It is interesting to consider the results of our study on the photochemistry of uracil, as its excited-state relaxation is also on the ultrafast vibrational time scale.

The results from this study and previous initial excited-state structural dynamics studies with uracil derivatives show that the methyl groups at the C5 and/or C6 positions determine the relative intensities of the 1235, 1310, and 1665 cm^{-1} modes.[14,15,18,29] Thus, the position of the methyl group plays an important role in determining the initial excited-state structural dynamics of uracil derivatives. A quick glance at Table 2 will give us an idea about the excited-state slopes for different vibrational modes. Although a mode-to-mode comparison of excited-state slopes is difficult, due to the change in PEDs and the modes themselves, comparing modes with similar mode description shows that the excited-state slopes are lower for the analogous mode in 5,6-DMU compared to the other uracil derivatives. However, the potential energy distributions (PEDs) and frequencies of the resonance Raman active modes change as the position of the methyl substitution changes, which make the molecular interpretation of the initial excited-state structural dynamics problematic.

Because it is difficult to compare the normal modes across the uracil derivatives, as the mode description and PEDs are different for different normal modes, we calculated the percentage distribution of total reorganization energy along different internal coordinates for the four uracil derivatives and tabulated these in Table 5. For calculation of the percentage distribution of reorganization energy along a particular internal coordinate for each normal mode the following equation is used

$$\%\ \text{reorganization energy} = \frac{\sum_{n}^{j=1}\left\{\left(\frac{\left(\frac{\beta}{\hbar}\right)^2}{2\bar{\nu}}\right)_j C_{ij}\right\}}{\sum_{n}^{j=1}\left(\frac{\left(\frac{\beta}{\hbar}\right)^2}{2\bar{\nu}}\right)_j} \times 100\% \tag{4}$$

where $((\beta/\hbar)^2/(2\bar{\nu}))$ is the reorganization energy for each normal mode, $\bar{\nu}$ is the vibrational frequency in cm^{-1}, c_{ij} is the percentage contribution of the ith internal coordinate to the corresponding jth normal mode (i.e., the PED % from Tables 1 and 2), and n is the total number of observed normal modes. Thus, the total fraction of reorganization energy along a particular internal coordinate is calculated by summing up all the individual reorganization energies along that particular internal coordinate and dividing by the total reorganization energy.

This analysis provides a new perspective on the initial excited-state structural dynamics of uracil derivatives. For uracil, 21% of the total reorganization energy lies along the C4O10 stretching coordinate, whereas for the methyl-substituted uracil derivatives, there is no reorganization energy along that internal coordinate. The percentage distribution of reorganization energy along the C=C bond is lowest for uracil and similar and higher for 6-MU, 5-MU, and 5,6-DMU. This suggests that the presence of a methyl substitution at the C5 or C6 position will channel the reorganization energy from the C4=O10 stretching mode to the C5=C6 stretching mode, changing the initial excited-state structural dynamics to modes that are more photochemically relevant. Unfortunately, the pyramidalization coordinate that is expected to be important as the C5 and C6 carbon atoms rehybridize is symmetry forbidden in resonance Raman spectroscopy. However, the in-plane bends may provide some small insight into the bond angle and dihedral angle changes happening at these two carbon centers in the first few femtoseconds. For the total in-plane bend coordinate, the percent reorganization energy is lowest for 6-MU and all other uracil derivatives have a larger and similar percentage of reorganization energy along this internal coordinate. However, when we look at the C5 and C6 in-plane bend coordinates separately, the reorganization energy is more or less the same along the C5 bend for all uracil derivatives. The C6 in-plane bend coordinate seems to have a larger difference in the distribution of reorganization energy than at C5, with the highest value for 5-MU and the lowest for 6-MU. It is clear from this analysis that methyl substitution at C5 and/or C6 affects the reorganization energy along the C6 in-plane bend coordinate. The percentage of total reorganization energy oriented along the photochemical coordinate is larger and similar for 5-MU and 5,6-DMU and least for uracil. For all ring stretching modes taken together, the percentage reorganization energy is higher in uracil and 6-MU compared to 5-MU or 5,6-DMU, and for ring deformation modes, the percentage distribution of reorganization energy is similar for all uracil derivatives. The higher percentage reorganization energy along the ring stretching modes in uracil and 6-MU indicates that the energy is distributed and delocalized into nonphotochemically relevant stretching modes, decreasing the localization of reorganization energy in the photochemically active coordinates.

It has been shown from experimental evidence[3] and calculations[3,30] that methyl substitution at C5 and C6 of uracil affects the electronic transition energy and the excited-state potential energy surface. The longer excited-state lifetime of

dx.doi.org/10.1021/jp412747c | J. Phys. Chem. A 2014, 118, 4680−4687

C5-substituted uracil compared to other derivatives indicates the importance of C5 substitution and its effect on electronic dynamics.[3] The difference in the initial excited-state structural dynamics of thymine and uracil has also been attributed to the presence of the C5 methyl group.[17] It is clear from Tables 1, 2, and 5 that the modes are more localized in methyl-substituted uracils. Similarly, the methyl groups seems to localize the vibrations involving the C5 and C6 centers in 5,6-DMU. This localization of vibrational energy and the change in the excited-state electronic transition in methyl-substituted uracils may affect the excited-state slopes which define the initial excited-state structural dynamics. The lower excited-state slopes observed in 5,6-DMU compared to the other uracil derivatives suggest that the excited-state geometry is not very different from the ground-state geometry. The observed decrease in the excited-state slope in 5,6-DMU compared to 5-MU, 6-MU, and U may be due to the higher number of vibrational degrees of freedom. Additionally, there could be geometrical constraints imposed by the methyl groups at the C5 and C6 positions which may restrict the molecule from excited-state geometry changes, resulting in the lower excited-state slopes in 5,6-DMU.

Whether there is a difference in the excited-state potential energy surface of thymine and uracil is still not clear. Gustavsson et al. suggested that such a difference exists and accounts for the difference in excited-state lifetime.[10] Yamazaki et al., however, found that the excited-state potential energy surface is similar for thymine and uracil in the gas phase, despite the observed difference in the excited-state lifetime.[31] They attributed the difference between the experimental excited-state lifetime and the calculated gas-phase potential energy surface to a solvent effect. It is already well established that the solvent interaction will affect the electronic potential energy surface of the nucleobases.[7,8] Our results here, along with previous studies from our group,[14,15,18] show that at least the initial excited-state slope of U, 5-MU, 6-MU, and 5,6-DMU are different. This difference in the initial excited-state geometry change compared to other uracil derivatives may change the nature of the excited-state potential energy surface where it meets the conical intersection.

Although the photochemistry of 5,6-DMU is not known, it is expected to be similar to thymine and uracil. Thymine and uracil form the cyclobutyl pyrimidine dimer, [6−4] photoproduct, and photohydrate but differ in the percentage yield of each.[1] The most intense modes in 5,6-DMU are assigned to dynamics around the C5 and C6 positions, similar to that observed in thymine, which are consistent with the expected photochemistry of 5,6-DMU. The C5═C6 lengthening and change in hybridization of the C5 and C6 carbons are expected in the $^1(\pi\pi^*)$ excited state which are also consistent with the expected photochemistry. Thus, higher excited-state slopes along the modes which have internal coordinates along the photochemically active coordinate suggest that the initial excited-state structural dynamics coincide with the expected photochemistry.

The similar electronic parameters in all uracil derivatives confirm the similarity between the electronic properties of uracil, 5,6-DMU, 5-MU, and 6-MU. Inhomogeneous broadening is mainly due to solvent−solute interactions, which are static within the dephasing time scale. The high inhomogeneous line width indicates that there is a broader solvent-induced zero−zero energy in 5,6-DMU compared to other methyluracils. This result is expected as the size of the molecule increases. Homogeneous broadening in the nucleobases is mainly due to solvent-induced dephasing, with a smaller contribution from population decay. The decrease in the homogeneous line width in 5,6-DMU compared to 5-MU and 6-MU is a little surprising. This decrease may arise from the steric protecting effect of the methyl group, which may decrease the solvent−solute collisions that lead to dephasing. Further studies on the excited-state lifetimes and their solvent dependence are required to better understand the broadening mechanisms.

■ CONCLUSIONS

The resonance Raman spectrum of 5,6-DMU is intermediate between that of 5-MU and 6-MU. The presence of a methyl group at the C5 and/or C6 positions determines the partitioning of the initial excited-state structural dynamics to favor photochemical CH bending and C═C stretching coordinates. The initial excited-state structural dynamics along the C5═C6 bond-lengthening coordinate are similar in all C5- or C6-substituted methyl uracil derivatives and different from uracil. The methyl substitution at the photochemical active centers redistributes the initial excited-state structural dynamics along photochemically active coordinates. The decrease observed in the calculated excited-state slopes for the different modes in 5,6-DMU compared to 5-MU and 6-MU can be attributed to the 5,6-DMU geometry constraint imposed by the two methyl groups and the increase in the number of vibrational degrees of freedom. This initial excited-state structural dynamics study has demonstrated that the excited-state potential energy surfaces of methyl uracil derivatives are different at least in the excited Franck−Condon region. Only further photochemistry experiments with 6-MU and 5,6-DMU to measure the yields of different photoproducts will enable us to establish the relationship between the initial excited-state structural dynamics and the photochemistry.

■ AUTHOR INFORMATION

Corresponding Author

*Phone: (780) 492-9704. E-mail: glen.loppnow@ualberta.ca.

Notes

The authors declare no competing financial interest.

■ REFERENCES

(1) Ruzsicska, B. P.; Lemaire, D. G. E. DNA photochemistry. In *CRC Handbook of Organic Photochemistry and Photobiology*; Horspool, W. H., Song, P.-S., Eds.; CRC Press: New York, 1995; pp 1289−1317.

(2) Shetlar, M. D.; Basus, V. J. The Photochemistry of Uracil: A Reinvestigation. *Photochem. Photobiol.* **2011**, *87*, 82−102.

(3) Gustavsson, T.; Banyasz, A.; Lazzarotto, E.; Markovitsi, D.; Scalmani, G.; Frisch, M. J.; Barone, V.; Improta, R. Singlet Excited-state Behavior of Uracil and Thymine in Aqueous Solution: A Combined Experimental and Computational Study of 11 Uracil Derivatives. *J. Am. Chem. Soc.* **2006**, *128*, 607−619.

(4) Merchan, M.; Gonzalez-Luque, R.; Climent, T.; Serrano-Andrs, L.; Rodraguez, E.; Reguero, M.; Pelaez, D. Unified Model for the Ultrafast Decay of Pyrimidine Nucleobases. *J. Phys. Chem. B* **2006**, *110*, 26471−26476.

(5) Hare, P. M.; Crespo-Hernandez, C. E.; Kohler, B. Internal Conversion to the Electronic Ground State Occurs via Two Distinct Pathways for Pyrimidine Bases in Aqueous Solution. *Proc. Natl. Acad. Sci. U.S.A.* **2007**, *104*, 435−440.

(6) Kwok, W. M.; Ma, C.; Phillips, D. L. Femtosecond Time- and Wavelength-resolved Fluorescence and Absorption Spectroscopic Study of the Excited States of Adenosine and an Adenine Oligomer. *J. Am. Chem. Soc.* **2006**, *128*, 11894−11905.

(7) Kleinermanns, K.; Nachtigalloa, D.; de Vries, M. S. Excited State Dynamics of DNA Bases. *Int. Rev. Phys. Chem.* **2013**, *32*, 308−342.
(8) Middleton, C. T.; de La Harpe, K.; Su, C.; Law, Y. K.; Crespo-Hernandez, C. E.; Kohler, B. DNA Excited-state Dynamics: From Single Bases to the Double Helix. *Annu. Rev. Phys. Chem.* **2009**, *60*, 217−239.
(9) Buchvarov, I.; Wang, Q.; Raytchev, M.; Trifonov, A.; Fiebig, T. Electronic Energy Delocalization and Dissipation in Single- and Double-stranded DNA. *Proc. Natl. Acad. Sci. U.S.A.* **2007**, *104*, 4794−4797.
(10) Barbatti, M.; Aquino, A. J. A.; Szymczak, J. J.; Nachtigallova, D.; Hobza, P.; Lischka, H. Relaxation Mechanisms of UV-photoexcited DNA and RNA Nucleobases. *Proc. Natl. Acad. Sci. U.S.A.* **2010**, *107*, 21453−21458.
(11) Pancur, T.; Schwalb, N. K.; Renth, F.; Temps, F. Femtosecond Fluorescence Up-conversion Spectroscopy of Adenine and Adenosine: Experimental Evidence for the $\pi\sigma^*$ State? *Chem. Phys.* **2005**, *313*, 199−212.
(12) Gustavsson, T.; Improta, R.; Markovitsi, D. DNA/RNA: Building Blocks of Life Under UV Irradiation. *J. Phys. Chem. Lett.* **2010**, *1*, 2025−2030.
(13) Kwok, W.-M.; Ma, C.; Phillips, D. L. A Doorway State Leads to Photostability or Triplet Photodamage in Thymine DNA. *J. Am. Chem. Soc.* **2008**, *130*, 5131−5139.
(14) Yarasi, S.; Brost, P.; Loppnow, G. R. Initial Excited-state Structural Dynamics of Thymine are Coincident with the Expected Photochemical Dynamics. *J. Phys. Chem. A* **2007**, *111*, 5130−5135.
(15) Yarasi, S.; Ng, S.; Loppnow, G. R. Initial Excited-state Structural Dynamics of Uracil from Resonance Raman Spectroscopy are Different from Those of Thymine (5-Methyluracil). *J. Phys. Chem. B* **2009**, *113*, 14336−14342.
(16) Billinghurst, B. E.; Yeung, R.; Loppnow, G. R. Excited-state Structural Dynamics of 5-Fluorouracil. *J. Phys. Chem. B* **2006**, *110*, 6185−6191.
(17) Ng, S.; Teimoory, F.; Loppnow, G. R. Mass-tuned Initial Excited-state Structural Dynamics of DNA Nucleobases from UV Resonance Raman Spectroscopy: 5-Deuterouracil. *J. Phys. Chem. Lett.* **2011**, *2*, 2362−2365.
(18) Teimoory, F.; Loppnow, G. R. Initial Excited-state Structural Dynamics of 6-Methyluracil: The Importance of Pyramidalization and Bond Lengthening Motions in its Photochemistry. To be submitted for publication.
(19) Billinghurst, B. E.; Loppnow, G. R. Excited-state Structural Dynamics of Cytosine from Resonance Raman Spectroscopy. *J. Phys. Chem. A* **2006**, *110*, 2353−2359.
(20) Myers, A. B. Excited Electronic State Properties from Ground-State Resonance Raman Intensities. In *Laser Techniques in Chemistry*; Myers, A. B., Rizzo, T. R., Eds.; Wiley: New York, 1995; pp 325−384.
(21) Kelley, A. M. Resonance Raman Intensity Analysis of Vibrational and Solvent Reorganization in Photoinduced Charge Transfer. *J. Phys. Chem. A* **1999**, *103*, 6891−6903.
(22) Lee, S.-Y.; Heller, E. J. Time-dependent Theory of Raman Scattering. *J. Chem. Phys.* **1979**, *71*, 4777−4788.
(23) Li, B.; Johnson, A. E.; Mukamel, S.; Myers, A. B. The Brownian Oscillator Model for Solvation Effects in Spontaneous Light Emission and Their Relationship to Electron Transfer. *J. Am. Chem. Soc.* **1994**, *116*, 11039−11047.
(24) Mukamel, S. *Principles of Nonlinear Optical Spectroscopy*; Oxford University Press: New York, 1995.
(25) Frisch, M. J.; Trucks, G. W.; Schlegel, H. B.; Scuseria, G. E.; Robb, M. A.; Cheeseman, J. R.; Scalmani, G.; Barone, V.; Mennucci, B.; Petersson, G. A.; et al. *Gaussian 09*, revision B.01.2009; Gaussian, Inc.: Wallingford, CT, 2010.
(26) Martin, J. M. L.; Van Alsenoy, C. *GAR2PED*; University of Antwerp: Antwerp, The Netherlands, 1995.
(27) Matsika, S.; Spanner, M.; Kotur, M.; Weinacht, T. C. Ultrafast Relaxation Dynamics of Uracil Probed via Strong Field Dissociative Ionization. *J. Phys. Chem. A* **2013**, *117*, 12796−12801.
(28) Schreier, W. J.; Schrader, T. E.; Koller, F. O.; Gilch, P.; Crespo-Hernandez, C. E.; Swaminathan, V. N.; Carell, T.; Zinth, W.; Kohler, B. E. Thymine Dimerization in DNA is an Ultrafast Photoreaction. *Science* **2007**, *315*, 625−629.
(29) Billinghurst, B. E.; Oladepo, S. A.; Loppnow, G. R. Initial Excited-state Structural Dynamics of Thymine Derivatives. *J. Phys. Chem. B* **2012**, *116*, 10496−10503.
(30) Hudock, H. R.; Levine, B. G.; Thompson, A. L.; Satzger, H.; Townsend, D.; Gador, N.; Ullrich, S.; Stolow, A.; Martınez, T. J. Ab Initio Molecular Dynamics and Time-resolved Photoelectron Spectroscopy of Electronically Excited Uracil and Thymine. *J. Phys. Chem. A* **2007**, *111*, 8500−8508.
(31) Yamazaki, S.; Taketsugu, T. Nonoradiative Deactivation Mechanisms of Uracil, Thymine and 5-Fluorouracil: A Comparative Ab Initio Study. *J. Phys. Chem. A* **2012**, *116*, 491−503.